Digital Communications and Networks 10 (2024) 1297–1304

Contents lists available at ScienceDirect

Digital Communications and Networks

journal homepage: www.keaipublishing.com/dcan

Performance comparison of single-carrier and multi-carrier waveforms over terahertz wireless channels

Dongxuan He [a], Zhi Zhang [b], Hao Lin [b], Zuomin Wu [b], Yingpei Huang [b], Zhaocheng Wang [a,c,*]

[a] Department of Electronic Engineering, Tsinghua University, Beijing 100084, China
[b] OPPO Research Institute, Beijing, China
[c] Tsinghua Shenzhen International Graduate School, Shenzhen 518055, China

ARTICLE INFO

Keywords:
Terahertz communication
RF imperfection
Single-carrier waveform
Multi-carrier waveform

ABSTRACT

Terahertz (THz) wireless communication has been recognized as a powerful technology to meet the ever-increasing demand of ultra-high rate services. In order to achieve efficient and reliable wireless communications over THz bands, it is extremely necessary to find an appropriate waveform for THz communications. In this paper, performance comparison of various single-carrier and multi-carrier waveforms over THz channels will be provided. Specifically, first, a system model for terahertz communication is briefly described, which includes amplifier nonlinearity, propagation characteristic, phase noise, etc. Then, the transceiver architectures related to both single-carrier and multi-carrier waveforms are presented, as well as their corresponding signal processing techniques. To evaluate the suitability of the waveforms, key performance metrics concerning power efficiency, transmission performance, and computational complexity are provided. Simulation results are provided to compare and validate the performance of different waveforms, which demonstrate the outstanding performance of Discrete-Fourier-Transform spread Orthogonal Frequency Division Multiplexing (DFT-s-OFDM) to THz communications when compared to Cyclic Prefix-OFDM (CP-OFDM) and other single-carrier waveforms.

1. Introduction

With emerging applications, such as Virtual-Reality (VR), Augmented Reality (AR), Digital Twin, Internet-of-Thing (IoT), etc., wireless communication is undergoing a revolution for higher data rate and lower latency. In particular, an ultra-high data rate in the range of Terabits per second (Tbps) is required in the era of Beyond Fifth-Generation (B5G), which has driven the urge to explore an expansion into new radio spectrum to meet user demands [1,2]. Terahertz (THz) band (0.1 THz-10 THz), which provides ultra broad bandwidth reaching tens or even hundreds of GHz, is capable of meeting the ever-increasing demand for ultra-high speed services. Therefore, THz communication has been envisioned as the key technology for B5G and Sixth-Generation (6G), which has been studied widely [3,4].

However, as the carrier frequency increases, THz signals tend to suffer from more severe transmission losses than their counterparts operating at lower-frequency, including both free space path-loss and molecular absorption loss [5]. In addition, the imperfections of Radio Frequency (RF) devices, due to the nonlinearity of Power Amplifier (PA) [6] and the Phase Noise (PN) of local oscillator [7], also pose great challenges to signal processing of THz communications. Therefore, much work remains to be done to facilitate the implementation of THz communications, such as waveform and coding design, beamforming optimization, etc. In particular, an appropriate waveform for THz communications is urgently needed to ensure both power efficiency and transmission performance. Aiming at the ultra-high data rate of THz communications, both the complexity and the performance of the candidate waveforms need to be carefully investigated.

As a type of waveform with convincing commercial success, Multi-Carrier (MC) waveforms including Orthogonal Frequency Division Multiplexing (OFDM) and Discrete-Fourier-Transform spread OFDM (DFT-s-OFDM) have received ever-increasing attention over years. Currently, OFDM and DFT-s-OFDM have already been adopted by the Third Generation Partnership Project (3GPP) due to their outstanding performance in frequency-selective fading channels. As a specific application scenario for THz communications, indoor transmission experiences a strong frequency-selective fading [8,9]. Therefore, MC waveforms are preferred candidates for THz communications and are considered in this work.

* Corresponding author at: Department of Electronic Engineering, Tsinghua University, Beijing 100084, China.
E-mail address: zcwang@tsinghua.edu.cn (Z. Wang).

https://doi.org/10.1016/j.dcan.2023.07.001
Received 5 January 2023; Received in revised form 22 June 2023; Accepted 2 July 2023
Available online 18 July 2023

Specifically, OFDM has been recognized as one of the most successful wireless communication waveform paradigms due to its superiority in handling multipath effects with low complexity. By decomposing a frequency selective channel into a set of independent and parallel subchannels, the frequency selective channel is converted into multiple flat channels, which makes one-tap Frequency Domain Equalizer (FDE) be capable of handling the adverse effect of channel fading [10,11]. In order to make the channel impulse response to be circularly convolved, a Cyclic Prefix (CP) is inserted before the transmitted symbols, which also acts as a guard interval to avoid Inter-Symbol Interference (ISI). However, some drawbacks of OFDM should be considered in its implementation, such as its sensitivity to frequency offset and high Peak-to-Average Power Ratio (PAPR).

Compared to CP-OFDM, DFT-s-OFDM has a better PAPR performance, which benefits from its DFT operation before subcarrier allocation [12]. Due to its flexible bandwidth allocation mechanism, DFT-s-OFDM can allocate different bandwidths to multiple users via frequency multiplexing. However, DFT-s-OFDM still suffers from low energy efficiency and severe nonlinear distortion, which is challenging for THz communications in the presence of PA nonlinearity.

To enable an energy-efficient transmission, a powerful candidate waveform for THz communication is the Single-Carrier (SC) waveform due to its low PAPR. In particular, SC-Quadrature Amplitude Modulation (SC-QAM) with Time Domain Equalization (TDE) is a kind of waveform with low PAPR and high spectral efficiency. However, the performance of TDE is limited when the channel is subject to strong frequency-selective fading, even with a receiver of high complexity. To solve this problem, FDE can be used to improve the transmission reliability. To ensure the effectiveness of the implementation of a simple FDE for the SC waveform, a simple solution is to insert CP into the waveform, similar to CP-OFDM [13,14]. As a result, the generated blocked SC-CP-FDE signals can be reliably demodulated at the receiver with relatively low complexity. Moreover, by replacing CP with Zero Padding (ZP) [15,16] to remove interblock interference, blocked SC-ZP-FDE signals can be easily handled by FDE, which will also be studied in this work.

In light of the above, we aim to present a comprehensive comparison of SC and MC waveforms for THz communications in the presence of RF imperfections. Specifically, a system model is presented for THz communications, where the channel propagation characteristics and the RF imperfections including PA nonlinearity and PN are considered. Then, the transceiver architectures and their corresponding signal processing techniques of SC-QAM, SC-CP-FDE, SC-ZP-FDE, CP-OFDM and DFT-s-OFDM are detailed. In addition, the key performance metrics of different waveforms are compared to find the most suitable waveform for THz communications. Simulation results demonstrate that the superiority of DFT-s-OFDM for THz communications when compared to other waveforms.

2. System model

In this paper, a THz channel model with realistic RF impairments is considered, including PA nonlinearity and phase noise. In particular, an end-to-end Single-Input Single-Output (SISO) THz communication system is considered, where both the transmitter and the receiver are equipped with one single antenna. An equivalent baseband model, where x is the complex-valued symbol to be transmitted, is used to model the THz transmission without loss of generality.

2.1. Amplifier nonlinearity

Before transmission, the THz signal x is first up-converted to the desired carrier frequency, and then amplified by PA. Since the path loss in THz channels is extremely high, PA is a critical device for THz systems that can efficiently guarantee the transmission distance. However, due to the nonlinearity of PA, the THz signal suffers from both amplitude compression and phase rotation, which significantly degrades the system performance [17]. In order to ensure transmission reliability, the PA can be operated away from its saturation region, which in turn reduces the power efficiency.

In this paper, the modified Rapp model, which is a quasi-memoryless nonlinear model adopted in 3GPP Radio Access Network (RAN) working group 1 (RAN1), is used to model the input and output signals of PA [18], where its Amplitude-to-Amplitude Modulation (AM-AM) and Amplitude-to-Phase Modulation (AM-PM) distortions can be respectively formulated as [19,20]

$$F_{AM-AM}(x_A) = \frac{Gx_A}{\left(1+|\frac{Gx_A}{V_{SAT}}|^{2p}\right)^{\frac{1}{2p}}} \tag{1a}$$

$$F_{AM-PM}(x_A) = \frac{Ax_A^q}{\left(1+|\frac{x_A}{V_B}|^{q}\right)} \tag{1b}$$

where x_A is the amplitude of the input signal x, G is the signal gain, V_{SAT} is the saturation level, p is the smoothness factor, and A, V_B and q are fitting parameters. Accordingly, the output of amplifier can be presented as

$$s = \frac{Gx_A}{\left(1+|\frac{Gx_A}{V_{SAT}}|^{2p}\right)^{\frac{1}{2p}}} \exp\left\{j\left(\theta + \frac{Ax_A^q}{\left(1+|\frac{x_A}{V_B}|^{q}\right)}\right)\right\} \tag{2}$$

where θ is the phase of input signal x.

2.2. Propagation characteristic

The amplified signal is then radiated through the THz channel. Typically, a multipath propagation model consisting of the Line-of-Sight (LoS) path and reflected rays, which can be used to represent the channel response of the THz channel, is given by [21,22]

$$h = \alpha_{\mathrm{LOS}}\delta(t-t_{\mathrm{LoS}})\mathcal{I}_{\mathrm{LOS}} + \sum_{q=1}^{N_{\mathrm{ref}}} \alpha_{\mathrm{ref}}^{q}\delta(t-t_{\mathrm{ref}}^{q}) \tag{3}$$

where $\mathcal{I}_{\mathrm{LoS}}$ is the indicator function for LoS path with $\mathcal{I}_{\mathrm{LoS}}=1$ indicating LoS case and $\mathcal{I}_{\mathrm{LoS}}=0$ indicating Non-LoS (NLoS) case, respectively. N_{ref} is the number of reflected rays, while α_{LoS} and t_{LoS} denote the attenuation and propagation delay of LoS path, respectively, and $\alpha_{\mathrm{ref}}^{q}$ and t_{ref}^{q} denote the attenuation and propagation delay of the q-th reflected path, respectively.

2.3. Phase noise

The phase noise, generated by the instability of Voltage-Controlled Oscillator (VCO) at both the transmitter and receiver, must be carefully evaluated. In particular, PN causes significant performance degradation in the form of phase rotation, which dramatically reduces the Signal-to-Interference plus Noise Ratio (SINR). Moreover, the PN increases with the square of the center frequency, which is not negligible in high-frequency THz transceivers. Considering the effect of PN, the n-th signal to be handled can be expressed as

$$y_n = r_n e^{j\Delta\theta_n} \tag{4}$$

where r_n is the n-th received signal, $\Delta\theta_n = \Delta\theta_{T,n} + \Delta\theta_{R,n}$ with $\Delta\theta_{T,n}$ and $\Delta\theta_{R,n}$ denoting PN generated by the transmitter and receiver, respectively.

To characterize the phase fluctuation, PN is commonly described in the frequency domain by its Power Spectral Density (PSD) in dBc/Hz, which is the ratio of the noise power measured in 1 Hz bandwidth to the power of the carrier at a given frequency offset [23]. In addition, the PSD of PN can be parameterized using multiple zero-pole equation, given by [24]

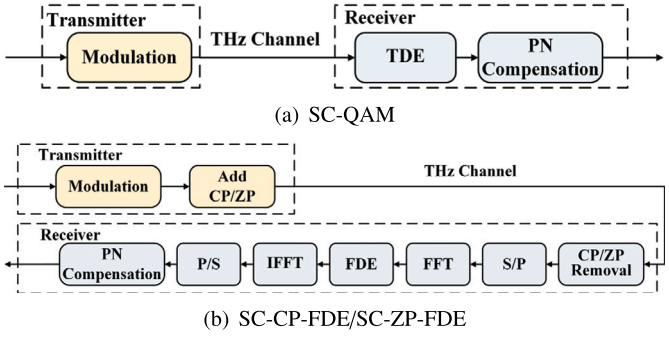

Fig. 1. Transceiver of SC waveforms.

$$S(f) = \mathrm{PSD}_0 \frac{\sum_{n=1}^{N}\left(1+(\frac{f}{f_{z,n}})^{\alpha_{z,n}}\right)}{\sum_{m=1}^{M}\left(1+(\frac{f}{f_{p,m}})^{\alpha_{p,m}}\right)} \tag{5}$$

where $S(f)$ is the single-sideband power spectral density of PN, f is the operation frequency that PN is measured, $f_{z,n}$ and $f_{p,m}$ are the zero frequency and pole frequency, respectively, and PSD_0 is the power spectral density for $f=0$ in dBc/Hz. $\alpha_{z,n}$ and $\alpha_{p,m}$ are the orders of zeros and poles, respectively.

3. Implementation of different waveforms

In this section, the implementation of different waveforms is presented, including the transceiver architecture and associated signal processing techniques.

3.1. Single-carrier transmission

Benefiting from their low PAPR, SC waveforms typically possess high PA efficiency and can be considered as a type of efficient waveform for THz communications. The following is a brief introduction to SC-QAM, SC-CP-FDE and SC-ZP-FDE.

3.1.1. SC-QAM

As shown in Fig. 1(a), SC-QAM transmitter sends QAM-modulated symbols $\mathbf{x}_{\text{SC-QAM}} = [x_0, \cdots, x_{L-1}]^{\mathrm{T}}$ into channel directly, where L is the number of transmitted symbols and $(\cdot)^{\mathrm{T}}$ denotes the transposition operation. At the receiver side, the TDE, which is realized by a Finite Impulse Response (FIR) filter, is used to process the received signal $\mathbf{y} = [y_1, \cdots, y_L]^{\mathrm{T}}$, given by

$$z_n = \sum_{m=0}^{L_{\mathrm{FIR}}-1} a_m y_{n-m} \tag{6}$$

where L_{FIR} and $\mathbf{a} = [a_0, \cdots, a_{L_{\mathrm{FIR}}-1}]$ are the length and coefficients of the FIR filter, respectively. Specifically, the filter response is designed to be the inverse of the channel response in order to reduce the channel frequency selectivity. Next, the PN compensation is adopted to handle the equalized signal $\mathbf{z} = [z_1, \cdots, z_L]$ before demodulation to ensure the reception performance.

3.1.2. SC-FDE

Although SC-QAM is easy to implement, its transmission performance is poor because the TDE cannot efficiently recover the received signal when the channel frequency selectivity becomes severe. To improve the performance, SC waveform with FDE (SC-FDE), whose transceiver architecture is shown in Fig. 1(b), can be regarded as a kind of reliable candidate for THz communication. Unlike SC-QAM, SC-FDE is a blockwise transmission scheme that can coordinate Fast Fourier Transform (FFT) operations at the receiver. Similar to MC waveforms, guard intervals including either CP or ZP are inserted into SC-FDE, which is beneficial to guarantee the effectiveness of FDE in the presence of channel multipath effects.

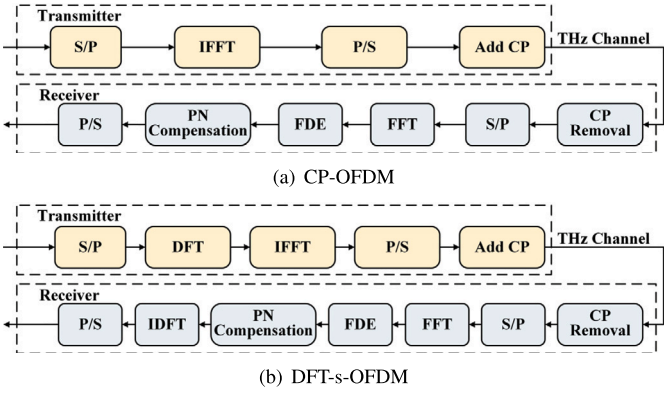

Fig. 2. Transceiver of MC waveforms.

Assuming that an N_{FFT}-point FFT operation will be performed at the receiver, the SC-CP-FDE symbol to be transmitted can be expressed as

$$\mathbf{x}_{\text{SC-CP-FDE}} = [\underbrace{x_{N_{FFT}-N_{\mathrm{CP}}}, \cdots, x_{N_{FFT}-1}}_{\text{Cyclic Prefix}}, x_0, \cdots, x_{N_{FFT}-1}]^{\mathrm{T}} \tag{7}$$

where N_{CP} is the length of CP.

At the receiver, the CP is first removed, and then, the received signal $\mathbf{y} = [y_0, \cdots, y_{N_{FFT}-1}]$ is transformed into frequency domain via FFT operation, given by $\mathbf{Y} = [Y_0, \cdots, Y_{N_{FFT}-1}]^{\mathrm{T}}$. In the frequency domain, simple one-tap Minimum Mean-Squared Error (MMSE) equalizer can efficiently reduce the frequency selectivity, which also significantly reduces the computational complexity of receiver. The FDE process can be formulated as $Z_k = G_k Y_k$, where G_k is obtained by

$$G_k = \frac{H_k^*}{|H_k|^2 + 1/SNR} \tag{8}$$

where $\mathbf{H} = [H_0, \cdots, H_{N_{FFT}-1}]^{\mathrm{T}}$ is the frequency response of THz channel. Subsequently, the recovered signal $\mathbf{Z} = [Z_0, \cdots, Z_{N_{FFT}-1}]$ is transformed into the time domain by Inverse Fast Fourier Transform (IFFT) operation. Before demodulation, PN compensation is executed to recover the phase rotation of signals.

Compared to SC-CP-FDE, the cyclic prefix is replaced by zero-padding in SC-ZP-FDE, which can be expressed as

$$\mathbf{x}_{\text{SC-ZP-FDE}} = [\underbrace{0, \cdots, 0}_{\text{Zero Padding}}, x_0, \cdots, x_{N_{FFT}-1}]^{\mathrm{T}} \tag{9}$$

At the receiver of SC-ZP-FDE system, the ZP is first removed. Next, a similar procedure as SC-CP-FDE is performed to process the received signal before demodulation.

3.2. Multi-carrier transmission

Compared to SC waveforms, MC waveforms offer higher spectral efficiency, more flexible resource allocation in the frequency domain, and easier integration with multiple antenna technologies, thus enabling them to be widely investigated. As two of the most successful examples, CP-OFDM and DFT-s-OFDM have been extensively studied and accepted by 3GPP.

3.2.1. CP-OFDM

CP-OFDM, as shown in Fig. 2(a), has been selected as both uplink and downlink waveforms in 5G due to its superior transmission

Table 1
Comparison of SC and MC waveforms.

	Pros	Cons
SC-QAM	Low PAPR and Adjacent Channel Leakage Ratio (ACLR) Allow asynchronous multiplexing Simple waveform synthesis	Limited spectral assignment flexibility Non-trivial support for MIMO High complexity TDE
SC-FDE	Similar Pros as SC-QAM Simple FDE implementation	Limited spectral assignment flexibility Non-trivial support for MIMO Less spectral efficiency than SC-QAM
CP-OFDM	Flexible frequency assignment Easy integration with MIMO Simple FDE to mitigate frequency selectivity	High ACLR-side lobe decays slowly Requires synchronous multiplexing
DFT-s-OFDM	Flexible bandwidth assignment Simple FDE implementation	Higher PAPR and lower ACLR than SC-QAM Requires synchronous multiplexing

performance and high spectral efficiency. A general CP-OFDM transmitter integrates Serial-to-Parallel (S/P) conversion, IFFT, Parallel-to-Serial (P/S) conversion, and CP insertion. CP is the part of the data concatenated at the beginning of an OFDM symbol that converts a linear convolution with the channel into a cyclic convolution. Therefore, the CP-OFDM symbol can be expressed as

$$\mathbf{x}_{\text{CP-OFDM}} = \left[\underbrace{x^{\text{OFDM}}_{N_{FFT}-N_{\text{CP}}}, \cdots, x^{\text{OFDM}}_{N_{FFT}-1}}_{\text{Cyclic Prefix}}, x^{\text{OFDM}}_{0}, \cdots, x^{\text{OFDM}}_{N_{FFT}-1}\right]^{\text{T}} \tag{10}$$

where $x_n^{\text{OFDM}} = \sum_{k=0}^{N_{FFT}-1} d_k e^{j2\pi f_k n T_s}$ with d_k denoting the QAM-modulated symbols to be transmitted, T_s is the sample interval, and f_k is the k-th carrier frequency. The duration of the CP, which should be longer than the maximum channel delay spread, is set according to the channel delay spread characteristics to eliminate ISI.

At the receiver, similar to the operation of SC-CP-FDE, the CP of the received signal is first removed, and then, the signal is transformed into the frequency domain by the FFT operation. Next, a simple linear MMSE equalizer can be used to restore the received signal by $Z_k = G_k Y_k$ and PN is then compensated before demodulation.

3.2.2. DFT-s-OFDM

Although CP-OFDM exhibits excellent transmission performance in the frequency-selective channel, its poor power efficiency limits its implementation in the uplink, especially in User Equipment (UE). To overcome this problem, DFT-s-OFDM, which adds a DFT block before subcarrier mapping, has been adopted in the uplink of Long Term Evolution (LTE). Benefiting from this DFT block, the resulting DFT-s-OFDM behaves like a DFT-based precoded SC waveform with a lower PAPR, thus increasing both the power efficiency and the coverage of the UE.

The transmitted symbol in a DFT-s-OFDM system can be expressed as a vector with N_{FFT} samples, defined by

$$\mathbf{x}_{\text{DFT-s-OFDM}} = \left[\underbrace{x^{\text{DFT}}_{N_{FFT}-N_{\text{CP}}}, \cdots, x^{\text{DFT}}_{N_{FFT}-1}}_{\text{Cyclic Prefix}}, x^{\text{DFT}}_{0}, \cdots, x^{\text{DFT}}_{N_{FFT}-1}\right]^{\text{T}} \tag{11}$$

where x_n^{DFT} is the n-th element of $\mathbf{x}^{\text{DFT}} = \mathbf{F\Delta Dd}$ with $\mathbf{d} = \left[d_1, d_2, \cdots, d_{N_{DFT}}\right]^{\text{T}}$ is an $N_{DFT} \times 1$ vector with N_{DFT} QAM-modulated symbols, $\mathbf{D}$ is the $N_{DFT} \times N_{DFT}$ matrix which performs N_{DFT}-point DFT operation, $\mathbf{\Delta}$ is the $N_{FFT} \times N_{DFT}$ mapping matrix for subcarrier assignment, and $\mathbf{F}$ performs N_{FFT}-point IFFT operation. At the receiver of DFT-s-OFDM, processing similar to CP-OFDM is adopted, where FDE with MMSE criterion can be used to compensate for frequency selective fading. Finally, PN compensation and IDFT are applied before demodulation.

In order to have a thorough comparison of different waveforms, Table 1 is presented, where the advantages and disadvantages of our considered SC and MC waveforms are compared.

It should be noted that, the direct application of CP-OFDM and DFT-s-OFDM to THz systems is challenging due to RF imperfections. On the one hand, considering the high PAPR of MC waveforms compared to SC waveforms, appropriate PAPR reduction algorithms are needed to mitigate the adverse effects of PA nonlinearity, which will help to improve the transmission efficiency. On the other hand, efficient PN estimation and compensation are also required due to the fact that MC waveforms are sensitive to phase noise. To address the above issues, more discussion on the compensation of RF imperfections will be presented.

3.3. Phase noise compensation

As an important performance degrading effect, PN needs to be compensated to ensure the transmission performance. PN compensation methods for SC and MC waveforms are studied, with respect to classical methods and their state-of-the-art improvements.

For SC waveforms, the PN typically performs as phase rotation of symbols, whose fast variations can be adaptively tracked in a decision-oriented manner [25]. In particular, a Phase-Tracking Reference Signal (PT-RS) can be inserted to track the phase, which allows the phase offset estimation and compensation in the time domain. Specifically, the difference between the original PT-RS and its received counterpart is calculated as [26]

$$\tilde{\theta} = \angle\left(\sum x^*_{PT,n} z_{PT,n}\right) \tag{12}$$

where $x_{PT,n}$ and $z_{PT,n}$ are the n-th original PT-RS and its received counterpart, respectively, and $(\cdot)^*$ and $\angle$ are the conjugate operation and the angle operation, respectively. Furthermore, PN is compensated by rotating $\mathbf{z}$ by $\tilde{\theta}$. To further improve the accuracy of the PN estimation, the received data symbols can also be used to estimate the phase noise. For example, an iterative algorithm is proposed in [27] to jointly compensate PN and detect data symbols, where decision data symbols are used to support the phase estimation and to track the change in PN.

For MC waveforms, which are more sensitive to phase noise, the distortion caused by phase noise will destroy the orthogonality between different subcarriers, resulting in DFT leakage [28]. In detail, PN will induce both Common Phase Error (CPE) and InterCarrier Interference (ICI) among different subcarriers, which represent the common rotation of all constellation points in the complex plane and additive Gaussian noise to different subcarriers, respectively [29]. Typically, based on the pilot, the CPE can be well estimated and then the symbols can be calibrated by dividing the received signals with the estimated CPE. However, the CPE compensation methods may not always be effective because they neglect the effect of ICI. To solve this problem, the ICI is usually approximated as a random Gaussian noise, whose energy is estimated, and a linear MMSE equalizer in the frequency domain is used to suppress the ICI [30,31].

In addition to the classic PN compensation methods described above, a great deal of work has been done to improve the performance of PN compensation. For a comprehensive understanding of the state-of-the-art PN compensation methods, Table 2 is presented.

Table 2
The existing PN compensation methods for SC-QAM, SC-FDE, CP-OFDM, and DFT-s-OFDM. (See [27,32–42].)

	Description
SC-QAM	[32] proposed a pilot based phase compensation method using smoothing technique is utilized to track the temporal dynamics of the phase noise. [33,34] proposed to use a Viterbi and Viterbi (V&V) method to compensate the PN, which is a kind of feedforward method. In [35], a decision-based maximum likelihood phase estimation method was proposed.
SC-FDE	[36] proposed an iterative decision-based compensation method. [27] combined the pilot-based and iterative decision-based compensation method to improve the compensation performance. [37] proposed to estimate and compensate the phase noise after each iteration of the iterative frequency-domain equalization.
CP-OFDM	[38] proposed to use MMSE equalization method to mitigate both CPE and ICI, where ICI is approximated as a Gaussian noise. In [39], decorrelator and interference canceler were used to mitigate the phase noise. [40] proposed to use the Karhunen-Loève representation of the phase noise process to estimate the phase noise in the time domain.
DFT-s-OFDM	[41] proposed to use cumulative sum filtering to estimate the phase noise. In [42] linear interpolation between pilot observations was used to estimate the phase noise, and then a projection in a discrete cosine transform basis and a Kalman filter were used to track the phase noise.

4. Key performance metrics

In this section, key performance metrics are presented in terms of power efficiency, transmission performance, and computational complexity.

4.1. PAPR and CM

As mentioned earlier, PA nonlinearity severely distorts the signal and thus adversely affects wireless communication systems. In particular, the envelope fluctuation of signals will result in inefficient use of PA or reduced transmission performance. To ensure the transmission performance, the average output power of the PA should be kept away from its saturation point to ensure that the PA operates in its linear region, called Output Back-Off (OBO). Typically, OBO is defined as the difference between the output saturation power and the average output power of the PA, given by

$$\mathrm{OBO} = 10\log_{10}\frac{p_{\mathrm{o,max}}}{p_{\mathrm{o,avg}}} \tag{13}$$

where $p_{\mathrm{o,max}}$ and $p_{\mathrm{o,avg}}$ are the maximum and average output power of PA, respectively.

With sufficient OBO, the transmission performance can be guaranteed at the cost of reduced power efficiency, which means that the OBO cannot be too large. To properly determine the OBO, the PAPR can be considered as a useful metric. Specifically, the PAPR, defined as the ratio of the peak power to the average power, is a rough indication of the envelope variations, given by

$$\mathrm{PAPR}(x) = \frac{\max|x|^2}{\mathbb{E}\left\{|x|^2\right\}} \tag{14}$$

where $\mathbb{E}\{\cdot\}$ is the expectation operation.

According to PAPR, the operating power can be accurately de-rated from its saturation region without redundant OBO, thus ensuring both power efficiency and transmission performance. However, PAPR cannot account for the amount of distortion caused by PA nonlinearity. In addition, the main cause of Adjacent Channel Leakage Ratio (ACLR) is the third-order nonlinearity caused by PA, which cannot be predicted by PAPR. To address this issue, the Cubic Metric (CM) is chosen as another performance metric with respect to PA nonlinearity, which takes into account the third-order nonlinearity of PA [43]. Typically, CM can be expressed as [44,45]

$$\mathrm{CM} = \frac{20\log_{10}\left\{rms|\overline{x}^3|\right\} - 20\log_{10}\left\{rms|\overline{x}_{ref}^3|\right\}}{K} \tag{15}$$

Table 3
Comparison of PAPR and CM.

	PAPR (dB)		RCM (dB)	
	QPSK	16QAM	QPSK	16QAM
SC-QAM	0	2.14	0	2.64
SC-CP-FDE	0	2.14	0	2.64
SC-ZP-FDE	0.27	2.42	0.54	2.42
CP-OFDM	8.56	8.56	7.71	7.69
DFT-s-OFDM	5.97	6.68	3.34	4.73

where $20\log_{10}\left\{rms|\overline{x}^3|\right\}$ is called Raw Cubic Metric (RCM), $20\log_{10}\left\{rms|\overline{x}_{ref}^3|\right\}$ is the raw cubic metric of the reference signal, $rms(\cdot)$ is the Root-Mean-Square (RMS) operation, $\overline{x}$ and $\overline{x}_{ref}$ are normalized waveform of x and reference signal x_{ref}, respectively, and K is an empirical factor.

The PAPR and RCM of 5 SC/MC waveforms with different modulations are listed in Table 3. It can be observed that SC waveforms have lower PAPR and RCM compared to MC waveforms, making them power efficient-suitable for coverage sensitive scenarios and extending the battery life of the UE. In addition, the PAPR (RCM) of SC-QAM is the same as that of SC-CP-FDE, since the CP is only a copy of the transmitted symbols. Nevertheless, the PAPR (RCM) of SC-ZP-FDE are slightly higher than those of SC-QAM and SC-CP-FDE because the zero padding operation reduces the average power, while it does not affect the peak power when compared to SC-QAM and SC-CP-FDE. Benefiting from the DFT block, the PAPR (RCM) of DFT-s-OFDM is lower than that of CP-OFDM. However, the PAPR (RCM) of DFT-s-OFDM is still relatively high when compared to SC waveforms.

4.2. Transmission reliability

As the most important key performance metric for wireless communication systems, it is imperative to compare the transmission reliability achieved by different waveforms. The transmission reliability of THz communications is challenging due to the severe path loss, multipath effects, and RF imperfections, which must be carefully studied.

To evaluate the transmission reliability, Bit Error Rate (BER), which is ratio of the number of error bits to the total number of bits, can be used to evaluate the transmission reliability. More results on the BER performance for different waveforms are presented in Section 5.

4.3. Computational complexity

Due to the ultra-high data rate of THz communications, low-complexity signal processing is required, which is another critical met-

Table 4
Complexity comparison of equalization for different waveforms.

Waveform	Computational Complexity	
SC-QAM	TDE:	$\mathcal{O}(N_{sym} \times L_{\mathrm{FIR}})$
SC-CP-FDE	FFT:	$\mathcal{O}(N_{\mathrm{FFT}} \times \log_2 N_{\mathrm{FFT}})$
	FDE:	$\mathcal{O}(N_{sym})$
SC-ZP-FDE	IFFT:	$\mathcal{O}(N_{\mathrm{FFT}} \times \log_2 N_{\mathrm{FFT}})$
CP-OFDM	FFT:	$\mathcal{O}(N_{\mathrm{FFT}} \times \log_2 N_{\mathrm{FFT}})$
	FDE:	$\mathcal{O}(N_{sym})$
DFT-s-OFDM	FFT:	$\mathcal{O}(N_{\mathrm{FFT}} \times \log_2 N_{\mathrm{FFT}})$
	FDE:	$\mathcal{O}(N_{sym})$
	IDFT:	$\mathcal{O}(N_{sym} \times \log_2 N_{sym})$

Table 5
Parameters of PA model [20].

Parameters	Values
Small Signal Gain	$G = 16$
Saturation Level	$V_{SAT} = 1.9$ V
Smoothness Factor	$p = 1.1$
Fitting Parameters	$A = -345$, $V_B = 0.17$, $q = 4$

Table 6
Parameters of PN model.

PSD_0	8894 (39.49 dB)			
n, m	$f_{z,n}$	$\alpha_{z,n}$	$f_{p,n}$	$\alpha_{p,n}$
1	3×10^3	2.37	0.7	3.2
2	120×10^3	2.8	330×10^2	3.2
3	900×10^6	2.4	17×10^6	1

ric for evaluating our considered waveforms. It is evident that the signal processing at the receiver is more complicated than at the transmitter, and the complexity of equalization dominates the computational complexity at the receiver. The computational complexity of equalization when N_{sym} symbols are transmitted is detailed in Table 4.

For SC-QAM, the complexity of equalization mainly lies on the TDE operation, which is determined by the number of taps in the FIR based equalizer, i.e., L_{FIR}. Since L_{FIR} becomes large when the channel frequency selectivity is severe, the computational complexity of the SC-QAM's receiver is high. As for waveforms using FDE, the computational complexity of equalization consists of FFT and the FDE operations. It can be seen that the complexity of FDE operation is relatively low, which is $\mathcal{O}(N_{sym})$ proportional to the number of symbols transmitted. Therefore, the FFT operation accounts for the dominant part of the computational complexity of the FDE-based receiver. It can be observed that, the computational complexity of SC-FDE and DFT-s-OFDM is about twice that of CP-OFDM, since both IFFT and IDFT are required by these two waveforms after equalization.

5. Numerical results

In this section, we present the simulation results to compare the transmission reliability of different waveforms with Quadrature Phase Shift Keying (QPSK) and 16QAM modulations over THz channels in the presence of PA nonlinearity and PN. In particular, the Clustered Delay Line (CDL) model in [46] is used to characterize the multipath THz channel, where CDL-B and CDL-D models are used to represent the NLoS and LoS scenarios, respectively. The RMS delay spread of the channel is set to be 10 ns, and the velocity of the UE is set to 3 km/h. In addition, the PA and PN models described in Section 2 are used, where the parameters of the PA and PN models are shown in Table 5 and Table 6, respectively. In addition, the THz transceiver is assumed to operate at 200 GHz with bandwidth $BW = 2$ GHz, and the length of each subblock is 2048. To ensure the effectiveness of transmission, OBO is set as 15 dB, and the length of CP and ZP are 128. In order to mitigate the adverse effects, the pilot-based and iterative decision-aided compensation method proposed in [27] is adopted to compensate the phase noise in SC waveforms, and the CPE method is used to compensate the phase noise in MC waveforms.

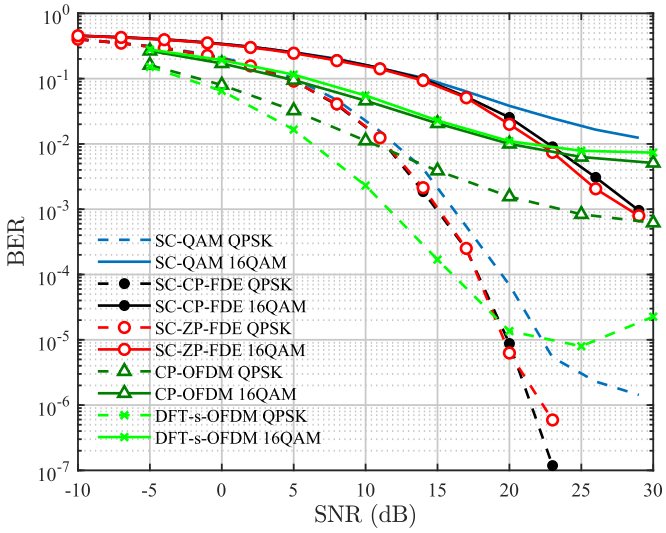

Fig. 3. Performance comparison of SC and MC waveforms over CDL-B channel.

In Fig. 3, we plot the BER versus SNR for different waveform schemes over CDL-B channel. It is clear that the BER performance deteriorates significantly with the increase of modulation order, indicating that high-order modulation is difficult to ensure the reliable transmission over the THz channel. Multipath effects, PA nonlinearities, and phase noise significantly degrade the quality of THz received signal, which cannot be effectively recovered. In addition, DFT-s-OFDM outperforms the other four types of waveforms. Specifically, when QPSK is considered, the DFT-s-OFDM has about 5 dB performance gain when compared to CP-OFDM, SC-CP-FDE, and SC-ZP-FDE and has 6 dB performance gain when compared to SC-OFDM at the BER of 10^{-2}. When 16QAM modulation is considered, the performance of DFT-s-OFDM, CP-OFDM, SC-CP-FDE, and SC-ZP-FDE tends to be the same at the BER of 10^{-2}, which has an over 10 dB performance gain when compared to SC-QAM. In addition, the SC-QAM has the worst BER performance regardless of the modulation because TDE cannot compensate the frequency selectivity when CDL-B channel is adopted.

In addition, there is an error floor for both CP-OFDM and DFT-s-OFDM due to their high PAPR. Although a 15 dB OBO back-off has been adopted, the maximum values of CP-OFDM and DFT-s-OFDM still operate in the nonlinear region of the PA, where they require more back-off to achieve a better transmission performance. In contrast, the BER performance of SC-QAM, SC-CP-FDE, and SC-ZP-FDE decreases monotonically with the increase of SNR, indicating that these SC waveforms can work at the linear region of PA when OBO = 15 dB. In terms of power efficiency, SC-QAM/SC-CP-FDE/SC-ZP-FDE have a clear advantage over DFT-s-OFDM/CP-OFDM.

In Fig. 4, BER performances for different waveforms over CDL-D channel for QPSK and 16QAM modulations are evaluated. It can be observed that a better BER performance can be achieved when compared to the results shown in Fig. 3. Unlike the CDL-B channel, the CDL-D channel has a distinct LoS path, which mitigates the frequency selectivity of the channel. As a result, even the SC-QAM can handle the channel frequency selectivity, where the BER performance of SC-QAM turns out to be the same as SC-CP-FDE and SC-ZP-FDE. In addition, the waveforms still achieve a better BER performance when compared to the SC waveforms. For example, DFT-s-OFDM and CP-OFDM have a 9 dB performance gain with QPSK modulation and over 10 dB performance gain with 16QAM modulation when compared to SC waveforms at the BER of 10^{-2}, which confirms the superiority of MC waveforms in our considered channel.

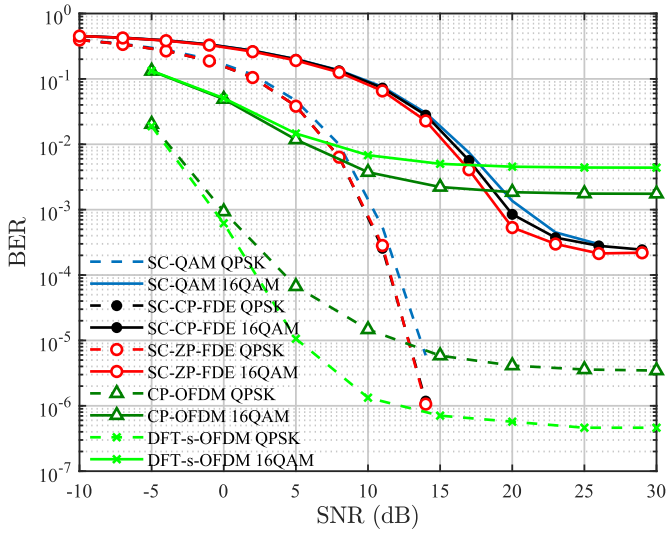

Fig. 4. Performance comparison of SC and MC waveforms over CDL-D channel.

In addition, the BER performance of SC waveforms becomes firstly worse and then better than that of MC waveforms in both Fig. 3 and Fig. 4, because the high PAPR of MC waveforms limits their transmission performance when OBO is insufficient. Therefore, it is difficult for MC waveforms to achieve a high SNR at a given noise power, because the high PAPR of MC waveforms requires a large OBO to ensure signal quality.

6. Conclusion

In this paper, we present a comprehensive comparison of single-carrier and multi-carrier waveforms for THz communications. Specifically, the single-carrier waveforms (exemplified by SC-QAM, SC-CP-FDE, and SC-ZP-FDE) and the multi-carrier waveforms (exemplified by CP-OFDM and DFT-s-OFDM) are included. In particular, a thorough comparison of different waveforms is provided in terms of power efficiency, computational complexity and transmission reliability. Simulation results show that DFT-s-OFDM outperforms other waveforms under severe frequency selective fading and RF imperfections. In addition, the multi-carrier waveforms are more sensitive to amplifier nonlinearity when compared to single-carrier waveforms.

Declaration of competing interest

The authors declare that they have no known competing financial interests or personal relationships that could have appeared to influence the work reported in this paper.

Acknowledgements

This work is supported in part by the National Key R&D Program of China under Grant 2018YFB1801501 and in part by the National Natural Science Foundation of China under Grant 62101306. This work is also supported by OPPO Research Fund.

References

[1] K. M, et al., Terahertz-enabled wireless system for beyond-5G ultra-fast networks: a brief survey, IEEE Netw. 33 (4) (2019) 89–95.
[2] I.F. Akyildiz, J.M. Jornet, C. Han, TeraNets: ultra-broadband communication networks in the terahertz band, IEEE Wirel. Commun. 21 (4) (2014) 130–135.
[3] Z. Chen, et al., A survey on terahertz communications, China Commun. 16 (2) (2019) 1–35.
[4] D. He, et al., Deep learning-assisted TeraHertz QPSK detection relying on single-bit quantization, IEEE Trans. Commun. 69 (12) (2021) 8175–8187.
[5] I.F. Akyildiz, C. Han, S. Nie, Combating the distance problem in the millimeter wave and terahertz frequency bands, IEEE Commun. Mag. 56 (6) (2018) 102–108.
[6] D. He, Z. Wang, Deep learning-assisted demodulation for terahertz communications under hybrid distortions, IEEE Commun. Lett. 26 (2) (2021) 325–329.
[7] E.N. Papasotiriou, A.-A.A. Boulogeorgos, A. Alexiou, Performance analysis of THz wireless systems in the presence of antenna misalignment and phase noise, IEEE Commun. Lett. 24 (6) (2020) 1211–1215.
[8] S. Priebe, M. Jacob, T. Kürner, Angular and RMS delay spread modeling in view of THz indoor communication systems, Radio Sci. 49 (3) (2014) 242–251.
[9] C. Lin, G.Y. Li, Distance-aware multi-carrier indoor terahertz communications with antenna array selection, in: Proceedings of 25th IEEE Annual International Symposium on Personal, Indoor, and Mobile Radio Communication (PIMRC), 2014, pp. 522–526.
[10] T. van Waterschoot, V. Le Nir, J. Duplicy, M. Moonen, Analytical expressions for the power spectral density of CP-OFDM and ZP-OFDM signals, IEEE Signal Process. Lett. 17 (4) (2010) 371–374.
[11] X. Ouyang, J. Zhao, Single-tap equalization for fast OFDM signals under generic linear channels, IEEE Commun. Lett. 18 (8) (2014) 1319–1322.
[12] A. Sahin, R. Yang, E. Bala, M.C. Beluri, R.L. Olesen, Flexible DFT-S-OFDM: solutions and challenges, IEEE Commun. Mag. 54 (11) (2016) 106–112.
[13] L. Deneire, B. Gyselinckx, M. Engels, Training sequence versus cyclic prefix-a new look on single carrier communication, IEEE Commun. Lett. 5 (7) (2001) 292–294.
[14] D. Falconer, et al., Frequency domain equalization for single-carrier broadband wireless systems, IEEE Commun. Mag. 40 (4) (2002) 58–66.
[15] Y.-S. Chen, C. Lin, Blind-channel identification for MIMO single-carrier zero-padding block-transmission systems, IEEE Trans. Circuits Syst. I, Regul. Pap. 55 (6) (2008) 1571–1579.
[16] R. Rajashekar, K.V.S. Hari, L. Hanzo, Spatial modulation aided zero-padded single carrier transmission for dispersive channels, IEEE Trans. Commun. 61 (6) (2013) 2318–2329.
[17] T.S. Rappaport, et al., Wireless communications and applications above 100 GHz: opportunities and challenges for 6G and beyond, IEEE Access 7 (2019) 78729–78757.
[18] 3GPP RP-160671, Study on New Radio Access Technology, NTT DOCOMO, INC.
[19] M. Honkanen, et al., New aspects on nonlinear power amplifier modeling in radio communication system simulations, in: Proceedings of 8th International Symposium on Personal, Indoor and Mobile Radio Communications, 1997, pp. 1–4.
[20] 3GPP R4-163314, Realistic power amplifier model for the New Radio evaluation, Nokia.
[21] C. Han, A.O. Bicen, I.F. Akyildiz, Multi-ray channel modeling and wideband characterization for wireless communications in the terahertz band, IEEE Trans. Wirel. Commun. 14 (5) (2015) 2402–2412.
[22] C. Han, I.F. Akyildiz, Distance-aware bandwidth-adaptive resource allocation for wireless systems in the terahertz band, IEEE Trans. THz Sci. Technol. 6 (4) (2016) 541–553.
[23] A. Hajimiri, T.H. Lee, A general theory of phase noise in electrical oscillators, IEEE J. Solid-State Circuits 33 (2) (1998) 179–194.
[24] 3GPP TR 38.808, Study on supporting NR from 52.6 GHz to 71 GHz, Release 17.
[25] A. Tarighat, R.C.J. Hsu, A.H. Sayed, B. Jalali, Digital adaptive phase noise reduction in coherent optical links, J. Lightwave Technol. 24 (3) (2006) 1269–1276.
[26] J. Feng, et al., Carrier phase estimation for 32-QAM optical systems using quasi-QPSK-partitioning algorithm, IEEE Photonics Technol. Lett. 28 (1) (2016) 75–78.
[27] Z. Sha, Z. Wang, Channel estimation and equalization for terahertz receiver with RF impairments, IEEE J. Sel. Areas Commun. 39 (6) (2021) 1621–1635.
[28] O. Edfors, M. Sandell, J.-J. van de Beek, S.K. Wilson, P.O. Borjesson, OFDM channel estimation by singular value decomposition, IEEE Trans. Commun. 46 (7) (1998) 931–939.
[29] Q. Zou, A. Tarighat, A.H. Sayed, Compensation of phase noise in OFDM wireless systems, IEEE Trans. Signal Process. 55 (11) (2007) 5407–5424.
[30] D. Petrovic, et al., Effects of phase noise on OFDM systems with and without PLL: characterization and compensation, IEEE Trans. Commun. 55 (8) (2007) 1607–1616.
[31] K. Nikitopoulos, S. Stefanatos, A.K. Katsaggelos, Decision-aided compensation of severe phase-impairment-induced inter-carrier interference in frequency-selective OFDM, IEEE Trans. Wirel. Commun. 8 (4) (2009) 1614–1619.
[32] Z. Zhang, S. Loh, S. Abu-Surra, R. Taori, Mitigation of phase noise and phase rotation in single-carrier communication systems using pilots and smoothing technique, in: Proceedings of IEEE International Conference on Ubiquitous Wireless Broadband (ICUWB), 2015, pp. 1–5.
[33] S.M. Bilal, G. Bosco, J. Cheng, A.P.T. Lau, C. Lu, Carrier phase estimation through the rotation algorithm for 64-QAM optical systems, J. Lightwave Technol. 33 (9) (2015) 1766–1773.
[34] J. Han, et al., Carrier phase estimation based on error function calculation for 16-QAM systems, IEEE Photonics Technol. Lett. 28 (22) (2016) 2561–2564.
[35] S. Zhang, P.Y. Kam, C. Yu, J. Chen, Laser linewidth tolerance of decision-aided maximum likelihood phase estimation in coherent optical M-ary PSK and QAM systems, IEEE Photonics Technol. Lett. 21 (15) (2009) 1075–1077.
[36] X. Cheng, N. Lou, B. Yuan, Iterative decision-aided compensation of phase noise in millimeter-wave SC-FDE systems, IEEE Commun. Lett. 20 (5) (2016) 1030–1033.

[37] Pedro, et al., Joint frequency domain equalisation and phase noise estimation for single-carrier modulations in doubly-selective channels, IET Commun. 9 (8) (2015) 1138–1146.
[38] S. Wu, Y. Bar-Ness, A phase noise suppression algorithm for OFDM-based WLANs, IEEE Commun. Lett. 6 (12) (2002) 535–537.
[39] S. Wu, P. Liu, Y. Bar-Ness, Phase noise estimation and mitigation for OFDM systems, IEEE Trans. Wirel. Commun. 5 (12) (2006) 3616–3625.
[40] A. Leshem, M. Yemini, Phase noise compensation for OFDM systems, IEEE Trans. Signal Process. 65 (21) (2017) 5675–5686.
[41] V. Syrjälä, T. Levanen, M. Valkama, Methods for phase noise mitigation for DFT-S-OFDM waveforms, in: Proceedings: IEEE Global Conference on Signal and Information Processing (GlobalSIP), 2016, pp. 660–664.
[42] J. Sibel, Pilot-based phase noise tracking for uplink DFT-s-OFDM in 5G, in: Proceedings 25th International Conference on Telecommunications (ICT), 2018, pp. 52–56.
[43] A. Behravan, T. Eriksson, Some statistical properties of multicarrier signals and related measures, in: Proceedings of IEEE 63rd Vehicular Technology Conference (VTC), 2006, pp. 1854–1858.
[44] 3GPP TSG RAN WG1, TDoc R1-060023, Cubic metric in 3GPP-LTE, Jan. 2006.
[45] K.-H. Kim, J.-S. No, D.-J. Shin, On the properties of cubic metric for OFDM signals, IEEE Signal Process. Lett. 23 (1) (2016) 80–83.
[46] 3GPP TR 38.901, Study on channel model for frequencies from 0.5 to 100 GHz, Release 16.